Mass measurements near the *r*-process path using the Canadian Penning Trap mass spectrometer

J. Van Schelt,[1,2] D. Lascar,[3,2] G. Savard,[1,2] J. A. Clark,[2] S. Caldwell,[1,2] A. Chaudhuri,[4,2] J. Fallis,[4,2] J. P. Greene,[2]
A. F. Levand,[2] G. Li,[5,2] K. S. Sharma,[4] M. G. Sternberg,[1,2] T. Sun,[2] and B. J. Zabransky[2]

[1]*Department of Physics, University of Chicago, Chicago, Illinois 60637, USA*
[2]*Physics Division, Argonne National Laboratory, Argonne, Illinois 60439, USA*
[3]*Department of Physics and Astronomy, Northwestern University, Evanston, Illinois 60208, USA*
[4]*Department of Physics, University of Manitoba, Winnipeg, Manitoba R3T 2N2, Canada*
[5]*Department of Physics, McGill University, Montréal, Québec H3A 2T8, Canada*

The masses of 40 neutron-rich nuclides from $Z = 51$ to 64 were measured at an average precision of $\delta m/m = 10^{-7}$ using the Canadian Penning Trap mass spectrometer at Argonne National Laboratory. The measurements, of fission fragments from a ^{252}Cf spontaneous fission source in a helium gas catcher, approach the predicted path of the astrophysical *r* process. Where overlap exists, this data set is largely consistent with previous measurements from Penning traps, storage rings, and reaction energetics, but large systematic deviations are apparent in β-endpoint measurements. Differences in mass excess from the 2003 Atomic Mass Evaluation of up to 400 keV are seen, as well as systematic disagreement with various mass models.

PACS number(s): 21.10.Dr, 27.60.+j, 27.70.+q, 26.30.Hj

I. INTRODUCTION

Neutron-rich isotopes have become increasingly more accessible to experiments requiring accelerated beams or trapped ions in recent years, and regions long unexplored are now being probed. Penning trap mass spectrometers are taking advantage of stopped fission and reaction products from gas catchers [1,2] and isotope separator on-line (ISOL) facilities [3–8] to give direct measurements of these nuclidic masses to high precision. The masses of nuclides far from stability are of interest for a variety of fields, including astrophysics and nuclear structure [9,10].

In particular, the rapid neutron-capture process (*r* process) [11–13] path is predicted to lie mostly in the region of unmeasured neutron-rich nuclides which is beginning to come into reach of precision study. Determination of neutron separation energies (S_n) from nuclear masses is critical for establishing the path of the *r* process, which is thought to lie near the line $S_n \approx 3$ MeV and is important for numerical simulations of *r*-process dynamics in different environments [14–16]. Much of the path is still inaccessible to experiment, but extending mass measurements closer to it provides information to better constrain mass models and extrapolations to the proposed *r*-process path and further still to the neutron drip line. Additionally, the appearance of neutron subshells, regions of deformation [5,17], and shell quenching [18] could be discovered via examination of S_{2n} trends.

Continuing a previous program of fission fragment mass measurements [1], the Canadian Penning Trap (CPT) at Argonne National Laboratory was used to measure the masses of 40 neutron-rich nuclides from $Z = 51$ to 64 near the target precision of $\frac{\delta m}{m} \approx 10^{-7}$, or $\delta m \approx 15$ keV/c^2. This paper reports on the results and techniques of those measurements and compares the results to previous measurements and the mass models on which *r*-process simulations depend.

II. EXPERIMENTAL PROCEDURE

The CPT and associated equipment have been described elsewhere [1,19], but details emphasizing recent additions relevant to these measurements will be presented here. The system, illustrated in Fig. 1, consists of a gas catcher for stopping reaction products, a radio-frequency quadrupole (RFQ) cooler and buncher, an isotope separator Penning trap, and a linear Paul trap for accumulation and staging of ions before injection in the precision Penning trap. Upgrades since the last CPT measurements in the neutron-rich region [1] include a larger-volume gas catcher with a stronger fission source and a higher-resolution isotope separator in a superconducting magnet.

The gas catcher [20] was designed to stop and cool ions produced either from an internal spontaneous fission source or from reactions using beams from the Argonne Tandem-Linac Accelerator System (ATLAS). This work was performed with fission fragments from a 150-μCi ^{252}Cf source placed behind a gold degrader foil with thickness optimized for collection of fragments in the heavy peak. The $\approx$ 1-m-length cylindrical gas catcher is filled with 50–70 torr of purified helium gas, which stops the fission products through collision and ionization. A large fraction, roughly 30%–50%, of these fission products stop as singly- or doubly-charged ions in the helium gas. An electrostatic gradient placed along the catcher axis pushes the ions toward the exit nozzle, while an rf ion guide [21] keeps the ions from touching the walls and neutralizing. At the downstream end the ion guide forms an rf funnel leading to the exit nozzle, where gas flow pushes the ions into the next stage.

Ions are carried away from the gas catcher nozzle by an RFQ ion guide [22] and are separated from the helium gas by the combined effects of electric fields and differential pumping. The ions are accumulated and bunched in a linear Paul trap at the end of the RFQ, where they are cooled further in $\approx 10^{-3}$ torr room-temperature helium gas. For these measurements, after 100 ms of accumulation the ion bunch
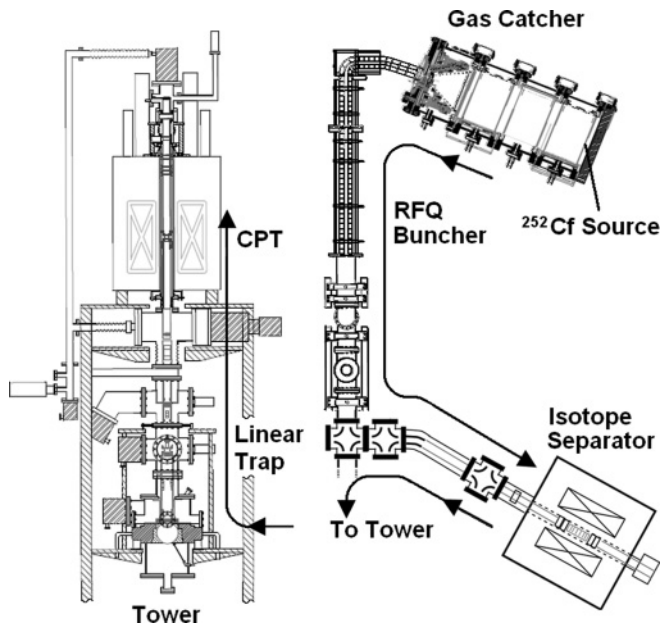
FIG. 1. Layout of the portion of the CPT system used in these measurements. Components are not to scale, and the CPT tower view has been separated from the rest of the system for convenience. Arrows indicate direction of ion travel.

is ejected from the trap into the beam line to the rest of the system.

Next, the ions are transferred to the isotope separator, where the ion bunches are purified. The isotope separator is a gas-filled cylindrical Penning trap [23] with a 2.25-T superconducting magnet. Penning traps allow two orbital motions of the trapped ions: the modified cyclotron motion with frequency ω_+ and the much slower magnetron motion with frequency ω_-, which are coupled by a cyclotron excitation $\omega_c = \omega_+ + \omega_- = qB/m$. In the isotope separator, all ions are pushed outward by a mass-insensitive rf dipole field driven at ω_- while the ions of interest are recentered in the trap by the application of a mass-sensitive rf quadrupole field at the ω_c frequency of those ions. The result is the accumulation of a purified sample of the desired ions with a mass resolving power of approximately 5×10^3 over the mass range studied here. This is sufficient to remove ions of different mass number as well as any hydrocarbon contaminants that may be at the same mass number. In cases where remaining molecular contamination is suspected, a strong dipole excitation at the reduced cyclotron frequency is applied to break up the molecules via gas collisions during the cleaning process. After cleaning, ions are transferred to a second linear Paul trap where multiple bunches from the isotope separator are accumulated and cooled before transfer to the precision Penning trap.

The CPT mass spectrometer consists of a hyperbolic Penning trap [24] in a highly stable 5.9-T magnetic field and ultra-high vacuum, where masses are measured using the time-of-flight technique [25]. The main electrodes approximate hyperboloids of revolution, with apertures in the endcaps for ion entry and ejection and a splitting of the ring electrode

into quadrants so that quadrupole excitations may be applied. Additional electrodes are placed between the endcaps and the ring to correct for the finite extent of the trap, and correction electrodes placed outside the endcaps prevent field penetration through the endcap apertures [25].

After an ion bunch is captured in this trap, the highest energy ions are evaporated away by briefly lowering the voltage of a correction tube and allowing them to escape. This is done both to keep only those ions which are in the region of the trap with the most homogeneous magnetic field and to decrease the ion time-of-flight spread. Any contaminants suspected to survive the isotope separator are then removed by a 100- to 300-ms dipole excitation at the ω_+ of those ions. Next, a dipole excitation at ω_- is applied for 40 ms to position the ions in an orbit with the desired radius.

The last step inside the Penning trap is the application of a quadrupole excitation at a candidate cyclotron frequency for 200 to 2000 ms. If the frequency applied matches the actual cyclotron frequency, the slow magnetron motion previously induced is converted to the much faster modified cyclotron motion at the same orbital radius [26]. A typical ω_+/ω_- ratio is 10^3, and thus the orbital kinetic energy increases by a factor of 10^6. After this final excitation the ion bunch is ejected from the trap and drifts down a $\approx$ 1-m long beam line to either a multichannel plate or channeltron time-of-flight detector outside the magnet. As the ions travel through the gradient of the main magnetic field, the orbital motion is converted adiabatically to linear motion, accelerating the ions down the line. Thus an application of a quadrupole field closer to the ion's true ω_c will result in a lower time of flight than a frequency farther away. By scanning frequencies over successive bunches of ions, the minimum in time of flight can be found, and a measurement of the the ion's ω_c made. Because the frequency is applied with a square-amplitude envelope, the time-of-flight spectrum reflects that envelope's Fourier transform: a sinc function. The cyclotron frequency of a calibrant ion of well-known mass is measured in the same manner, and the ratio of the frequencies is taken to cancel out the magnetic field term. The mass of the neutral atom is then given by the calibrant mass and frequency ratio, with additional terms to compensate for the charge states and the masses of electrons not present given the charge states:

$$m = \frac{\omega_{c(\text{cal})}}{\omega_c} \frac{q}{q_{\text{cal}}} (m_{\text{cal}} - q_{\text{cal}} m_e) + q m_e,$$

where the subscript "cal" refers to the calibrant, q is the integer charge state, and m_e is the mass of the electron. Alternatively, if multiple calibrant species are used, those frequency measurements can be combined as a single magnetic field strength measurement via $B = \omega_c m/q$, which can then be used to determine the unknown masses from their cyclotron frequency measurements. In either case, the calibrations need to be taken only as frequently as is required to monitor magnetic field drift, rather than after every measurement of an unknown ion. Atomic binding energies are small enough to be neglected for these measurements. Example time-of-flight scans are shown in Fig. 2.
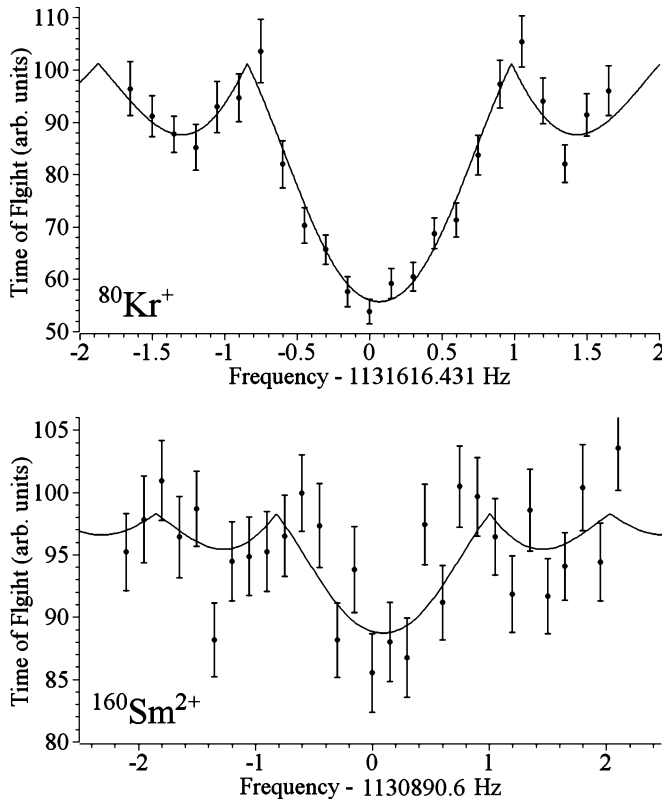
FIG. 2. Two example cyclotron frequency scans from the CPT, for the calibrant ^{80}Kr$^+$ and ion of interest, ^{160}Sm^{2+}. Both excitations are 1 s long, and the fit function is a modified sinc function which approximates the true time-of-flight curve [27]. The depth of the fit is less for the ^{160}Sm^{2+} scan because contaminant ions present in the Penning trap were not affected by the excitation.
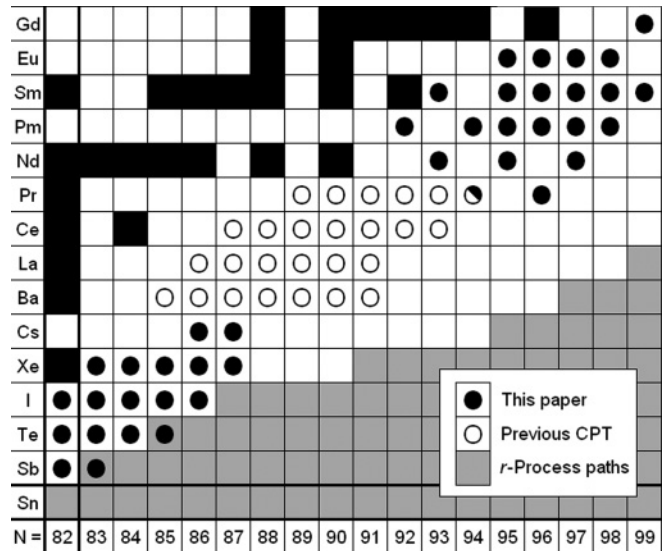

FIG. 3. Positions of measured nuclides on the chart of the nuclides. Nuclides marked with filled circles are those presented in this paper, and those with open circles were previously measured by the CPT mass spectrometer [1]. The shaded area represents the span of several possible *r*-process paths [13].

III. MEASUREMENTS

Following fission-fragment measurements made with a smaller gas catcher and source and a previous isotope separator [1], a new series of measurements in the ^{252}Cf fission heavy peak began in April 2008. The nuclides studied, identified in Fig. 3, can be divided into two components: the heaviest nuclides, from Pr to Gd, were measured in the 2^+ charge state over four weeks from April to July 2008; the lighter nuclides in the heavy peak, from Sb to Cs, were measured in the 1^+ charge state over four weeks in February and March 2009. High charge states are advantageous for mass measurements because their higher cyclotron frequencies lead to lower uncertainties in mass for the same uncertainty in frequency. However, due to interactions with the helium gas used to stop and cool the ions in preparation for the precision Penning trap, they are limited to only 1^+ or 2^+ in practice. The division of charge states in these measurements is due to the high ionization potential at the Xe electron shell closure, which allows the fission fragments with $Z \geq 56$ to survive as 2^+, but not those with $Z < 56$.

Excitation times used for candidate cyclotron frequencies range from 200 to 2000 ms, depending on the lifetime of the nuclide being studied and the conditions inside the trap. The total duration of each measurement—typically 1 to 30 h—was dictated by the target precision of one part in 10^7, the yield of ions out of the gas catcher, and the ultimate purity of the

sample in the Penning trap. To calibrate the 2^+ measurements, which range in mass-to-charge ratio from 76.5 to 81.5 $\frac{u}{e}$, the cyclotron frequencies of ^{12}C$_6^1$H$_4^+$, ^{80}Kr$^+$, and ^{86}Kr$^+$ were measured approximately once per measurement week, and all of the calibration measurements were combined to give a single value for the magnetic field. For the 1^+ measurements, ^{136}Xe$^+$ was measured at least once per measurement week. In all weeks but one, at least one calibration resonance was taken with identical excitation time as used in that period to determine the fitting-function parameters to be used. For ^{136}I, no calibration was taken with the same excitation time as the measurement because of an unplanned interruption in the experiment. To calibrate this 2000-ms measurement, the results of a 1000-ms calibration were used, and the width of the resonance was scaled from that calibration fit. Table I lists the mass values used for each calibrant, and Tables II and III list the cyclotron frequency ratios of each measured ion to each calibration ion.

After the first week of 1^+ measurements, an electrical discharge occurred in or near the precision Penning trap. A lasting result of this discharge was an additional trap

TABLE I. Mass values used for magnetic field calibrations. For the molecule, the mass listed is that of the ion plus the mass of an electron. The noble gas masses are those of neutral atoms. Relative weights are given for the influence of each calibrant's mass on the corresponding set of measurements: ^{136}Xe$^+$ for the 1^+ and the others for 2^+.

Calibrant	Mass used (u)	Source	Relative weight
^{136}Xe$^+$	135.907 214 484(11)	[28]	100%
^{12}C$_6^1$H$_4^+$	76.031 300 085 82(43)	[29–32]	18%
^{80}Kr$^+$	79.916 3790(16)	[29]	49%
^{86}Kr$^+$	85.910 610 73(11)	[29]	33%

TABLE II. Ratios of the cyclotron frequencies of the ions of interest to those of the ^{136}Xe$^+$ ions for measurements made in the 1$^+$ charge state. The calibrant mass used is listed in Table I.

Ion	ω_c ratio	Excitation time (ms)
^{133}Sb$^+$	1.022 510 200(79)	1000
^{134}Sb$^+$	1.014 832 72(27)	500
^{134}Te$^+$	1.014 904 071(49)	1000
^{135}Te$^+$	1.007 342 824(75)	1000
^{136}Te$^+$	0.999 905 180(37)	1000
^{137}Te$^+$	0.992 562 30(13)	1000
^{135}I$^+$	1.007 391 356(62)	1000
^{136}I$^+$	0.999 944 000(36)	2000
^{137}I$^+$	0.992 617 351(65)	1000
^{138}I$^+$	0.985 386 600(46)	1000
^{139}I$^+$	0.978 266 90(22)	1000
^{137}Xe$^+$	0.992 664 183(83)	1000
^{138}Xe$^+$	0.985 447 843(42)	1000
^{139}Xe$^+$	0.978 321 228(81)	1000
^{140}Xe$^+$	0.971 309 239(75)	1000
^{141}Xe$^+$	0.964 381 577(69)	1000
^{141}Cs$^+$	0.964 427 61(15)	1000
^{142}Cs$^+$	0.957 603 370(75)	1000

imperfection, possibly due to some surface charge deposited on a trap electrode. Resonances taken under these conditions show an asymmetry, the effect of which had to be mitigated

in the analysis as described below. A study undertaken with various stable Xe isotopes [33] found a systematic effect of only 0.37(33) $\frac{\text{keV}}{\text{u}}$ under these conditions, which is well below the statistical uncertainties in these measurements.

Most time-of-flight spectra were fit with a modified sinc function, which includes a parameter accounting for the possible over- or under-conversion from the ω_- to ω_+ motions [27]. For the data taken in the week following the discharge the time-of-flight spectrum showed an asymmetry in the side bands, pulling the modified sinc fit to the low-frequency side. A Gaussian function was used to fit that week's data to minimize this problem, and the uncertainties were appropriately inflated due to the increased χ^2 of these fits. In all cases, cuts were placed on the number of detected ions from a single ion bunch to minimize systematic effects discussed below.

There are several possible sources of systematic error, the largest of which are listed here. As the magnetic field drifts, ω_c will change, but the 5.9-T superconducting magnet is extremely stable (Fig. 4), with the field drift measured to be 0.1(0.4) ppb/day over a two-month period. Effects of trap misalignment and electric field imperfections are suppressed to high order [34]. In the weeks following the aforementioned discharge, the measured ω_c value for ^{136}Xe$^+$ drifted up 0.3(0.6) ppb/day as the trap recovered. This small potential source of error during this time was mitigated by using a calibration taken within one week of each measurement to calculate the mass. The ion cloud's charge alters the electric field of the trap, but the effect on the ω_c value has been measured to be <2.5 ppb per detected ion under normal conditions [33]

TABLE III. Ratios of the cyclotron frequencies of the ions of interest to those of the calibration ions for measurements made in the 2$^+$ charge state. The calibrant masses and relative weights used are listed in Table I. Uncertainties are those of calibrant and target ion combined.

| Ion	ω_c ratios			Excitation time (ms)
	$^{76}(^{12}\text{C}_6\,^1\text{H}_4)^+$	^{80}Kr$^+$	^{86}Kr$^+$	
^{153}Pr^{2+}	0.994 302 50(26)	1.045 110 12(27)	1.123 500 53(29)	200
^{155}Pr^{2+}	0.981 425 59(20)	1.031 575 21(22)	1.108 950 41(23)	500
^{153}Nd^{2+}	0.994 342 931(34)	1.045 152 616(32)	1.123 546 210(39)	500
^{155}Nd^{2+}	0.981 472 30(11)	1.031 624 31(11)	1.109 003 19(12)	500
^{157}Nd^{2+}	0.968 925 46(29)	1.018 436 35(30)	1.094 826 04(32)	200
^{153}Pm^{2+}	0.994 366 01(15)	1.045 176 87(16)	1.123 572 28(17)	500
^{155}Pm^{2+}	0.981 503 965(56)	1.031 657 596(57)	1.109 038 971(63)	500
^{156}Pm^{2+}	0.975 190 689(43)	1.025 021 719(42)	1.101 905 358(48)	1000
^{157}Pm^{2+}	0.968 964 141(81)	1.018 477 002(84)	1.094 869 742(92)	500
^{158}Pm^{2+}	0.962 807 82(15)	1.012 006 10(16)	1.087 913 48(17)	500
^{159}Pm^{2+}	0.956 733 59(11)	1.005 621 48(12)	1.081 049 97(13)	500
^{155}Sm^{2+}	0.981 526 10(15)	1.031 680 86(16)	1.109 063 98(17)	500
^{157}Sm^{2+}	0.968 993 178(51)	1.018 507 523(52)	1.094 902 552(58)	500
^{158}Sm^{2+}	0.962 848 141(58)	1.012 048 482(58)	1.087 959 039(65)	1000
^{159}Sm^{2+}	0.956 770 122(65)	1.005 659 884(67)	1.081 091 252(74)	200 & 500
^{160}Sm^{2+}	0.950 775 181(67)	0.999 358 608(69)	1.074 317 338(76)	1000
^{161}Sm^{2+}	0.944 844 874(74)	0.993 125 271(77)	1.067 616 458(84)	500
^{158}Eu^{2+}	0.962 861 30(15)	1.012 062 31(16)	1.087 973 91(17)	500
^{159}Eu^{2+}	0.956 794 898(63)	1.005 685 926(64)	1.081 119 248(71)	500
^{160}Eu^{2+}	0.950 795 89(10)	0.999 380 38(11)	1.074 340 74(12)	500
^{161}Eu^{2+}	0.944 877 14(11)	0.993 159 19(12)	1.067 652 92(13)	500
^{163}Gd^{2+}	0.933 275 822(91)	0.980 965 055(94)	1.054 544 14(10)	500
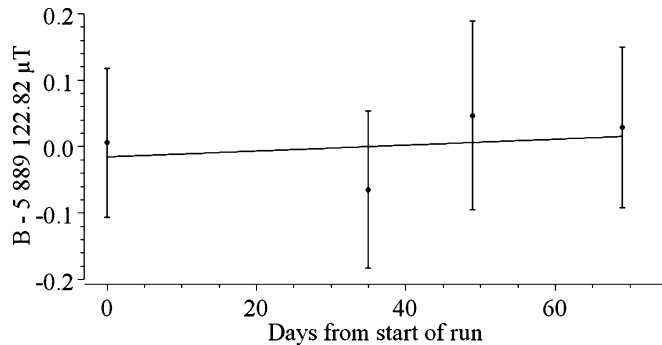
FIG. 4. Results of magnetic field calibration data taken over the span of the 2^+ measurements. Each point represents the combined result over all calibration species taken during the respective measurement weeks. The linear fit to these data gives a field drift of 0.1(0.4) ppb/day. The consequence of this negligible drift is that no systematic correction nor uncertainty were necessary. Note that not all weeks in this span contain mass measurements, but only those weeks for which calibrations are shown here.

and <17 ppb per detected ion with the post-discharge effect during these measurements. This effect will be suppressed if the trap population during measurement and calibration are kept low, as was the case here with the average number of detected ions per ejection ranging from 0.03 to 3.1 for the ions of interest and below 7 for the calibration ions. Contaminant ions of similar mass can have a separate effect as the ion motions interfere with each other. Based on a 100-ppb limit at 15 ions [35], we estimate the effect to have an upper limit of 10 ppb for the three-ion maximum rate here. The reference frequency used by the ω_c signal generator was compared to a Rb frequency standard and measured to be stable to 3 ppb over a two-week period. Mass-dependent effects in the precision Penning trap were investigated as part of a very high precision study of Xe isotopes [33]. A frequency-dependent attenuation of the applied ω_c amplitude was found at -0.1%/kHz over the frequency range, corresponding to A/q from 113 to 165. This, combined with a measured ω_c centroid dependence on amplitude due to the dodecapole moment of the trap, gives a variation of $-0.3 \frac{\text{keV}}{\text{u}}$, which is again mitigated by using calibrants of similar mass. Because these potential sources of error are much smaller than our statistical uncertainties of at least 32 ppb, or more typically 100 ppb, no systematic uncertainty was added to the quoted results.

IV. DISCUSSION

Of the 40 nuclides measured, 8 had been measured previously by Penning traps, 20 by β-endpoint only, and 3 had no previous mass measurement of any kind. Measurement uncertainties in the CPT results range from 5 to 46 μu, with most below or near the target 10^{-7} fractional uncertainty. Isomers with lifetimes long enough to be captured in the trap are not expected for any of the measured nuclides except ^{134}Sb [36,37] and ^{136}I [38], for which the identities of the measured states are unclear.

Table IV shows the new CPT measurements and compares them to the 2003 Atomic Mass Evaluation (AME03) [29]

as well as some more recent measurements [3,7,40]. The overall trend of these measurements versus the AME03 is of increasing mass as distance from stability increases, as seen in Fig. 5. This effect was also seen in the CPT's previous measurements of Ba, La, Ce, and Pr fission fragments [1], proton-rich nuclides of Nb to Rh [39], as well as measurements by other Penning traps [5–7]. Because the source data for the AME and its extrapolations are mostly from β-endpoint measurements, the observed deviations suggest an unaddressed systematic problem with that technique. The frequency of such disagreement suggests that β-endpoint results as a whole should not be trusted as a reliable source of data for extrapolations.

A. Comparison with past measurements

The trends evident in Fig. 5 demand separate comparisons between the CPT and literature mass values for different measurement techniques. Four categories have been selected for individual discussion below; these are grouped so that systematic trends in differences may be identified and each method evaluated for accuracy. Following these is a brief comparison of each new CPT measurement with the literature values for that nuclide.

1. Penning traps

Some of the masses measured here have been previously measured in the ISOLTRAP or CPT Penning traps. These are ideal checks on the accuracy of the experiment as a whole. The CPT had previously measured and published the mass of ^{153}Pr [1], and the present measurement is in agreement. ISOLTRAP has measured isotopic chains of Cs [3] and Xe [7] from proton-induced fission at ISOLDE to neutron numbers beyond the current reach of the CPT for these elements. Figure 6 shows a comparison between the seven nuclides measured by both traps, and there is no evidence of any systematic or isolated differences, with $\chi^2/6 = 0.9$. On average, the reported ISOLTRAP masses are $0.61(67)\sigma$ lower than the CPT masses.

2. Storage rings

The FRagment Separator–Experimental Storage Ring (FRS-ESR) [40] cooler-storage ring at GSI uses isochronous mass spectrometry to measure masses of fission products in a radioactive beam via time of flight. Eight nuclides of Sb, Te, I, and Xe have been measured at both the FRS-ESR and the CPT, and these are compared in Fig. 7. The two methods are in rough agreement but there is some scatter with an rms difference of 158 keV, despite the 120-keV uncertainty typical of the FRS-ESR results. Comparing the two data sets yields $\chi^2/7 = 1.8$, giving a statistical p value of 3%.

If this large scatter is a real effect, then—given the strong consistency of the Penning traps discussed above—it may be due to a flaw in either the FRS-ESR experiment or calibrant mass values. This latter possibility is a significant one, given that some of those calibrant masses are largely determined via β-endpoint measurements. Unfortunately, not enough information is given in the FRS-ESR publication [40] to accurately recalculate new mass values with updated calibrant masses and compare to the CPT results.

TABLE IV. Mass measurement results from the CPT. Results are given as the masses of neutral atoms. Sb through Cs were measured in the 1^+ charge state, while Pr through Gd were measured in the 2^+ state. Also listed are the mass excesses from the AME03 [29], the differences between the CPT and AME03 values, and the measurements from ISOLTRAP [3,7] and FRS-ESR [40].

Nuclide	Mass (u) CPT	Mass excess (keV)				
		CPT	AME03	$\Delta_{\text{CPT-AME03}}$	ISOLTRAP	FRS-ESR
^{133}Sb	132.915 277(10)	−78 918.7(9.5)	−78 943(25)	24(27)		−78 986(120)
^{134}Sb[a]	133.920 812(35)	−73 763(33)	−74 170(40)	407(52)		
^{134}Te	133.911 3976(65)	−82 532.6(6.0)	−82 559(11)	26(13)		−82 758(121)
^{135}Te	134.916 550(10)	−77 733.2(9.3)	−77 830(90)	97(90)		−77 725(123)
^{136}Te	135.920 1024(50)	−74 424.2(4.6)	−74 430(50)	6(50)		
^{137}Te	136.925 622(18)	−69 282(17)	−69 560(120)	280(120)		−69 290(120)
^{135}I	134.910 0503(82)	−83 787.6(7.7)	−83 790(7)	2(10)		
^{136}I[a]	135.914 8257(49)	−79 339.3(4.5)	−79 500(50)	161(50)		
^{137}I	136.918 0282(90)	−76 356.2(8.3)	−76 503(28)	147(29)		−76 518(121)
^{138}I	137.922 7265(64)	−71 979.8(6.0)	−72 330(80)	350(80)		
^{139}I	138.926 506(31)	−68 460(29)	−68 840(30)	380(42)		−68 527(121)
^{137}Xe	136.911 569(11)	−82 373(11)	−82 379(7)	6(13)	−82 382.2(1.8)	
^{138}Xe	137.914 1550(59)	−79 964.1(5.5)	−80 150(40)	186(40)	−79 975.1(3.3)	
^{139}Xe	138.918 791(11)	−75 645(11)	−75 644(21)	−1(24)	−75 644.6(2.1)	
^{140}Xe	139.921 658(11)	−72 976(10)	−72 990(60)	14(61)	−72 986.5(2.3)	−72 870(121)
^{141}Xe	140.926 785(10)	−68 199.5(9.4)	−68 330(90)	130(90)	−68 197.3(2.9)	−68 521(127)
^{141}Cs	140.920 058(21)	−74 466(19)	−74 477(11)	11(22)	−74 475(15)[c]	
^{142}Cs	141.924 303(11)	−70 511(10)	−70 515(11)	4(15)	−70 521(15)[c]	
^{153}Pr[b]	152.933 895(15)	−61 576(14)	−61 630(100)	54(100)		
^{155}Pr	154.940 508(32)	−55 416(30)	−55 780(300)#	360(300)#		
^{153}Nd	152.927 7156(47)	−67 332.5(4.4)	−67 349(27)	16(27)		
^{155}Nd	154.933 134(17)	−62 285(16)	−62 470(150)#	190(150)#		
^{157}Nd	156.939 383(46)	−56 464(43)	−56 790(200)#	330(200)#		
^{153}Pm	152.924 167(24)	−70 638(22)	−70 685(11)	47(25)		
^{155}Pm	154.928 1350(85)	−66 941.8(7.9)	−66 970(30)	28(31)		
^{156}Pm	155.931 1155(64)	−64 165.5(5.9)	−64 220(30)	54(31)		
^{157}Pm	156.933 119(13)	−62 299(12)	−62 370(110)	70(110)		
^{158}Pm	157.936 563(24)	−59 091(23)	−59 090(130)	0(130)		
^{159}Pm	158.939 284(19)	−56 557(17)	−56 850(200)#	290(200)#		
^{155}Sm	154.924 642(24)	−70 196(22)	−70 197.2(2.6)	1(22)		
^{157}Sm	156.928 4166(80)	−66 679.5(7.4)	−66 730(50)	50(51)		
^{158}Sm	157.929 9497(91)	−65 251.5(8.5)	−65 210(80)	−42(80)		
^{159}Sm	158.933 215(10)	−62 209.6(9.7)	−62 210(100)	0(100)		
^{160}Sm	159.935 333(11)	−60 237(10)	−60 420(200)#	180(200)#		
^{161}Sm	160.939 158(12)	−56 674(12)	−56 980(300)#	310(300)#		
^{158}Eu	157.927 791(25)	−67 262(23)	−67 210(80)	−52(83)		
^{159}Eu	158.929 100(10)	−66 043.2(9.5)	−66 053(7)	10(12)		
^{160}Eu	159.931 849(17)	−63 482(16)	−63 370(200)#	−110(200)#		
^{161}Eu	160.933 662(19)	−61 793(18)	−61 780(300)#	0(300)#		
^{163}Gd	162.934 175(16)	−61 316(15)	−61 490(300)#	170(300)#		

[a]Identity of measured state is ambiguous due to the possible presence of an isomer.
[b]Combined CPT result with value from [1]. See Sec. IV A 5 for details.
[c]Result has been adjusted due to a change in the calibration value since the publication of [3]. See Sec. IV A 5 for details.
#Extrapolated mass value.

3. Transfer and capture reactions

Five of the masses presented here had previously been established from nucleon-transfer or neutron-capture experiments. The (n, γ) reaction offers an opportunity for exquisitely precise neutron-separation energy (S_n) measurements due to the monoenergetic γ rays and the state of γ-ray absorption detector technology. $S_n(^{137}\text{Xe})$ has been measured to a precision of 80 eV by this method [41], in agreement with the CPT result. $S_n(^{155}\text{Sm})$ has twice been measured to
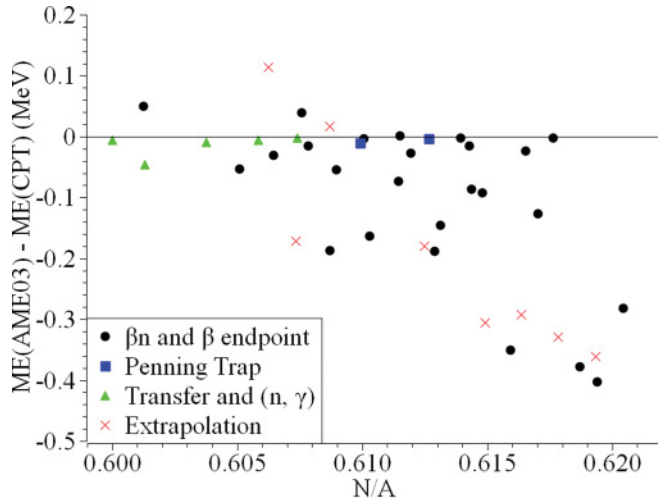
FIG. 5. (Color online) The difference between mass excess values from the AME03 [29] and CPT results. The horizontal axis was chosen to illustrate the increase in deviation with distance from stability. For each nuclide, the measurement technique most heavily weighted in the AME03 is indicated by the symbol used for each point. In cases where data from multiple techniques were used the most heavily weighted technique is indicated. Error bars are omitted for clarity; β-endpoint uncertainties range from 11 to 153 keV, Penning trap uncertainties are 11 keV, transfer and capture uncertainties range from 2.6 to 11 keV, and extrapolated mass uncertainties range from 150 to 300 keV.

sub-keV precision [42,43] and these are consistent, both with each other and with the CPT result.

Transfer reactions offer similar benefits, and four such measurements have been made on nuclides presented here. The mass of ^{135}I has been measured via ^{136}Xe$(d,^{3}$He) [44], ^{153}Pm via ^{154}Sm$(d,^{3}$He) [45] and ^{154}Sm(t,α) [46], and ^{159}Eu via ^{160}Gd(t,α) [47], to precisions of 40, 25, 20, and 8 keV/c^2, respectively. The differences between these and the CPT measurements, using AME03 mass values for the Sm and Gd parent nuclides, are 0.02, 0.12, 1.5, and 1.2σ, respectively, confirming the accuracy and reliability of transfer reaction measurements.

FIG. 7. (Color online) Comparison of CPT and FRS-ESR mass excess values [40]. In some cases the CPT error bars are smaller than the points.

4. β-endpoint measurements

β-endpoint measurements dominate the AME03 on the neutron-rich side of stability because of the applicability of that kind of measurement with a small number of nuclei. For 15 of the nuclides presented here where isomeric states are not suspected, the β-decay Q values can be calculated entirely from these CPT measurements, and a total of 22 β-endpoint measurements exist of these nuclides. A comparison of these data sets shows a systematic problem with the β-endpoint method, as illustrated in Fig. 8. Of the 22 measurements, 10 are within 1σ and another 6 within 2σ, but a long tail exists up to 9σ. Comparison of the data sets gives $\chi^2/21 = 10.7$, which has a statistical p value of 6×10^{-36}. Of the 22 β-endpoint measurements, 17 had values of Q_β smaller than the CPT results, which gives support to the notion that feeding to higher-lying states is erroneously pushing these measurements to lower masses.

Two recent sets of measurements demonstrate the importance of considering systematic uncertainties in β-endpoint experiments. Hayashi *et al.* [48] give new Q_β measurements for some of the Eu and Gd nuclides presented here and a new analysis of that group's earlier Pm and Sm [49,50] measurements, and Fogelberg *et al.* [51] measured Q_β for
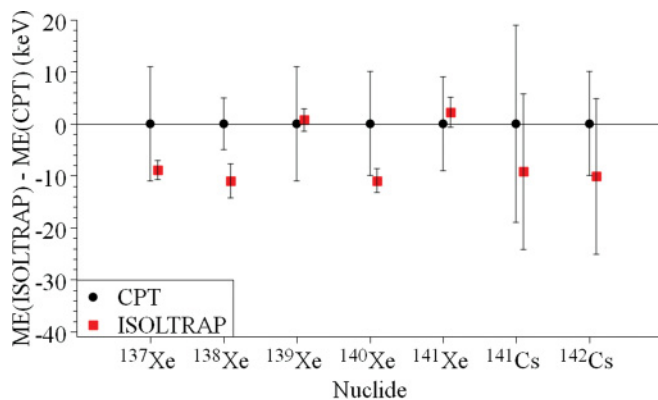

FIG. 6. (Color online) Comparison of CPT and ISOLTRAP mass excess values for Xe [7] and Cs [3] isotopes. No significant individual or systematic differences are seen.
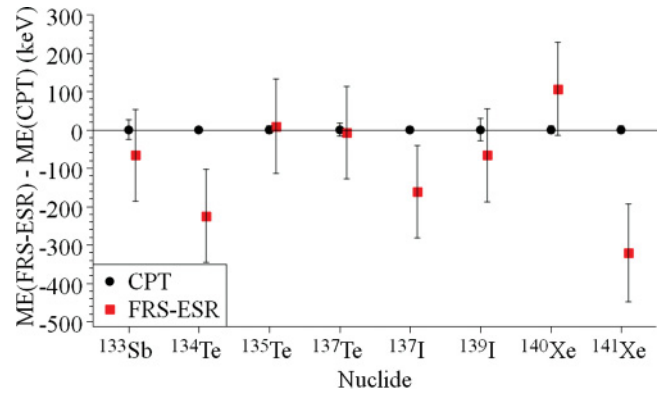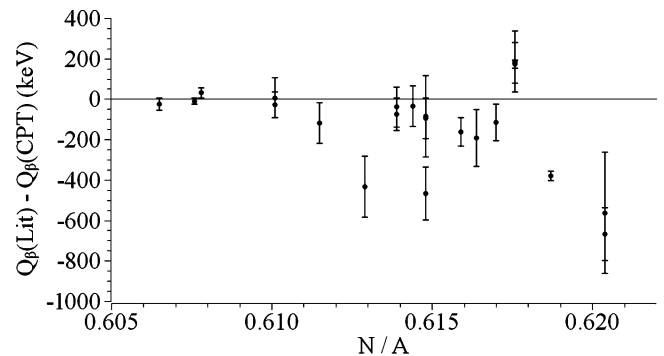

FIG. 8. Comparison of Q_β values as determined by β-endpoint measurements and CPT mass measurements of parent and daughter masses. The apparent trend is to more negative difference in the β-endpoint measurements with distance from stability. The outlier from this trend at $N/A = 0.618$ is ^{136}Te.

neutron-rich Te and I isotopes. The CPT results have good statistical agreement with the Hayashi *et al.* results, but less so with Fogelberg *et al.*, where deviations up to 9σ are seen. However, Fogelberg *et al.* report only a statistical uncertainty, and if the 100-keV systematic uncertainty suggested by Shibata *et al.* [52] and used by Hayashi *et al.* for the root-plot analysis method is applied, the disagreements decrease to less than 2σ.

5. Discussion by nuclide

What follows is a comparison to previous measurements of each nuclide presented here, ordered by element.

^{133}**Sb:** The AME03 cites a single experiment for the mass of ^{133}Sb, a β-endpoint measurement [53]. The value of Q_β in that paper is 4.002(7) MeV, leading to an evaluated mass excess of $-78.943(25)$ MeV. This is consistent with the CPT value of $-78.9187(95)$ MeV. A more recent experiment by the FRS-ESR facility measured ^{133}Sb via time of flight and reported a mass excess of $-78.986(120)$ MeV [40], which is also consistent with the CPT value.

^{134}**Sb:** There is a metastable state of ^{134}Sb with a 10-s lifetime and excitation energy estimated at 250 keV [36], and with a measurement from γ coincidence at 279 keV [37]. Only one resonance was observed with the CPT in the expected mass region, so the state of the measured ions is unclear. If the two states are within 400 keV of each other they would not be separately resolved in the CPT given the excitation time of 500 ms, so the observed resonance may be some weighted average of the two states.

The AME03 cites two β-endpoint measurements for the mass determination of ^{134}Sb: $Q_\beta = 8.390(45)$ MeV [54] and 8.420(120) MeV [55], both of which are significantly lower (6.9 and 2.8σ) than the CPT value of 8.769(34) MeV. If the measured state is assumed to be the metastable state, then a combination of the CPT measurement and the β-endpoint measurements above gives an excitation energy of 379(56) keV. We do not offer an assignment of the measured state.

^{134}**Te:** A single β-endpoint measurement is cited by the AME03 with $Q_\beta = 1.513(7)$ MeV [53], leading to a mass excess of $-82.559(11)$ MeV. This is marginally consistent with our result of $-82.5326(60)$ MeV. The FRS-ESR measurement gives $-82.758(121)$ MeV [40], a 1.9σ difference from the CPT result.

^{135}**Te:** Two β-endpoint measurements were used in the AME03 to calculate the mass excess of ^{135}Te: $Q_\beta = 5.960(100)$ MeV [55] and 5.970(200) MeV [56]. These are combined in the AME03 to give 5.960(90) MeV, consistent with the value from CPT measurements of 6.054(12) MeV. The recent FRS-ESR result gives a mass excess of $-77.725(123)$ MeV [40], which is consistent with the CPT value of $-77.7332(93)$ MeV.

A β-endpoint result by Fogelberg *et al.* [51] more recent than the AME03 gives $Q_\beta = 5.888(13)$ MeV, a 9.4σ difference from the CPT result. It is important to note that there was no systematic uncertainty assigned to that Q_β measurement, only a statistical one. Other authors [52] suggest a 100-keV systematic uncertainty for the root-plot method employed in that study. Increasing the Fogelberg *et al.* uncertainty to 100 keV reduces the disagreement to 1.6σ.

^{136}**Te:** Three measurements are used by the AME03 to determine this mass. The determination is dominated by a β-delayed neutron-emission Q-value measurement of $Q_{\beta n} = 1.285(50)$ MeV [57], which agrees with the CPT value of 1.292(9) MeV. The other citations are of β-decay Q-value measurements of $Q_\beta = 5.095(100)$ MeV [55] and 5.100(150) MeV [58]. If we assume that the CPT ^{136}I measurement is of the ground state (see discussion below) then both of these are somewhat higher than the CPT result of 4.915(7) MeV.

Since the AME03 publication, a new β-endpoint measurement has been made with $Q_\beta = 5.086(20)$ MeV [51], a disagreement of 171 keV and 8.1σ with the CPT result. Adding a 100-keV systematic uncertainty to the β-endpoint method as discussed above decreases the inconsistency to 1.7σ.

^{137}**Te:** Two β-endpoint experiments are cited in the AME03 for ^{137}Te: $Q_\beta = 7.030(300)$ MeV [56] and 6.925(130) MeV [55]. These are combined in the AME03 to 6.940(120) MeV, marginally consistent with the CPT result of 7.074(19) MeV. The AME03 mass excess value of $-69.560(120)$ MeV is 278 keV lower than our value of $-69.282(17)$ MeV. Over half of this difference, 147 keV, comes from the difference between the mass of ^{137}I used by the AME03 and that determined in our experiment, discussed below. The recent FRS-ESR measurement agrees with the CPT, with mass excess $-69.290(120)$ MeV [40].

^{135}**I:** In the AME03, two different methods primarily constrain the ^{135}I mass: a β-endpoint measurement of $Q_\beta = 2.627(6)$ MeV [53] and a $Q(^{136}\text{Xe}(d,^3\text{He})^{135}\text{I})$ measurement of $-4.438(40)$ MeV [44]. The CPT ^{135}I measurement gives $Q_{(d,^3\text{He})}(^{136}\text{Xe}) = -4.437(8)$ MeV, in excellent agreement with the AME03 input value. There is also a slight contribution to the ^{135}I mass in the AME03 from a ^{136}Te $Q_{\beta n}$ measurement [57] of 1.285(50) MeV, consistent with CPT's 1.292(9) MeV. The CPT results cannot be directly compared to the Q_β measurement.

^{136}**I:** There is a metastable state of ^{136}I [38] which, with the ground state, is expected to be produced in fission. Only one resonance was clearly measured during this experiment, and its identity is uncertain. If the states lie within 100 keV of each other they would not have been resolved given the excitation time of 2000 ms. The determination of the number of states trapped by the CPT was made difficult by the possible presence of $^{135}\text{Xe}^1\text{H}^+$ less than 1 Hz (200 keV) away from the observed ^{136}I or ^{136}I^m resonance. Because the mass of $^{135}\text{Xe}^1\text{H}^+$ is well known we can be certain that the resonance measured is not that molecule. The mass excess of the observed ^{136}I state is found to be $-79.3393(45)$ MeV, and Q_β is 7.0898(45) MeV.

The AME03 cites three papers for a total of four measurements of ^{136}I and its metastable state, each a β-endpoint measurement. The most recent of those [55] gives $Q_\beta = 6.925(70)$ and 7.705(120) MeV for the two states. An older paper [59] was disregarded for its measurement of the ground-state Q_β value, but its measurement of 7.100(230) MeV assigned to the isomer state was included in the evaluation. A third paper [60] gives only the ground state Q_β value at 6.960(100) MeV. The adopted AME03 Q_β values are 6.930(50) MeV for the ground state and 7.580(110) MeV for the metastable state.

These suggest that it is the ground state which was measured here; however, a paper published since the AME03 claims β-endpoint measurements of both the ground and metastable states, with $Q_\beta = 6.850(20)$ and $7.051(12)$ MeV [51], respectively. This is the same paper discussed above which did not include systematic uncertainties. Given the conflicting measurements it is difficult to assign a state to the measured ion.

^{137}**I:** The AME03 cites a β-delayed neutron study for this mass determination, with $Q_{\beta n} = 1.850(30)$ MeV [57]. The CPT measurement gives $Q_{\beta n} = 2.001(8)$ MeV, which disagrees by 5σ. Disregarded by the AME03 is a β-endpoint measurement of $Q_\beta = 5.880(60)$ MeV [55], which is inconsistent with the CPT result of $6.017(14)$ MeV. The recent FRS-ESR measurement gave a mass excess of $-76.518(121)$ MeV [40], which differs from the CPT result of $-76.3562(83)$ MeV by 1.3σ.

^{138}**I:** Only one experiment is cited in the literature for ^{138}I, a β-endpoint measurement of $Q_\beta = 7.820(70)$ MeV [55], a 2.3σ difference from our value of $7.984(7)$ MeV. The AME03 mass excess value of $-72.330(80)$ MeV disagrees with the CPT value of $-71.9798(60)$ MeV, a larger 4.4σ 350-keV difference. Of this difference, 186 keV is accounted for by our disagreement on the mass of ^{138}Xe discussed below.

^{139}**I:** A single previous measurement was available for the AME03, a β-endpoint measurement that gives $Q_\beta = 6.806(23)$ MeV [61], a 379-keV, 9.8σ difference from the CPT result of $7.185(31)$ MeV. Curiously, both the ^{139}Xe and ^{139}I Q_β measurements that the AME03 relies upon are in this same paper but have wildly different agreement with our results. The recent FRS-ESR mass excess result of $-68.527(121)$ MeV [40] agrees with the CPT result of $-68.460(29)$ MeV.

^{137}**Xe:** By virtue of the adjacency of ^{137}Xe to the stable ^{136}Xe, the mass of ^{137}Xe can be derived quite precisely from (n, γ) measurements. The AME03 cites such a measurement in a draft IAEA Technical Document. That document has since been published, with $S_n = 4025.53(8)$ keV [41], consistent with the CPT result of $4015(11)$ keV.

Another Penning trap, ISOLTRAP, recently measured all xenon isotopes from $A = 136$ to 146 with similar precision as these measurements [7]. The reported ISOLTRAP mass excess for ^{137}Xe of $-82.3822(18)$ MeV is in agreement with the CPT value of $-82.373(11)$ MeV.

^{138}**Xe:** Two β-endpoint measurements are used for the mass determination by the AME03. Those results are $Q_\beta = 2.720(50)$ MeV [62] and $2.830(80)$ MeV [63]. These are combined in the AME03 to give the adopted value of $2.740(40)$ MeV. As the mass of ^{138}Cs was not measured in our experiment, a calculation of Q_β entirely from CPT data is not possible. It was previously measured by ISOLTRAP, however, with an adjusted mass excess of $-82.887(13)$ MeV [3] (see ^{141}Cs, below, for adjustment). Combining these two Penning-trap measurements gives $Q_\beta = 2.923(14)$ MeV: a 183-keV 4.3σ disagreement.

ISOLTRAP's recent measurement of ^{138}Xe with mass excess $-79.9751(33)$ MeV [7] differs from the CPT value of $-79.9641(55)$ MeV by 1.7σ.

^{139}**Xe:** Two experiments have measured Q_β for this nuclide and are used by the AME03: $5.020(60)$ MeV

[63] and $5.062(22)$ MeV [61], averaged in the AME03 to $5.057(21)$ MeV. Using the adjusted mass excess value of ^{139}Cs from ISOLTRAP of -80.704 MeV [3] (see ^{141}Cs, below, for adjustment), our $Q_\beta = 5.059(17)$ MeV is consistent. The recent ISOLTRAP measurement of the ^{139}Xe mass excess is $-75.6446(21)$ MeV [7], which is also consistent with the CPT value of $-75.645(11)$ MeV.

^{140}**Xe:** There is only one existing Q_β measurement for ^{140}Xe, of $4.060(60)$ MeV [63]. Using the adjusted ISOLTRAP ^{140}Cs mass excess result of -77.046 MeV [3] (see ^{141}Cs, below, for adjustment), the CPT $Q_\beta = 4.070(13)$ MeV agrees with this. The CPT mass excess of $-72.976(10)$ MeV is consistent with both the ISOLTRAP measurement of $-72.9865(23)$ MeV [7] and the FRS-ESR measurement of $-72.870(121)$ MeV [40].

^{141}**Xe:** This xenon isotope also has a single Q_β measurement, with $Q_\beta = 6.150(90)$ MeV [63]. The CPT result of $Q_\beta = 6.266(21)$ MeV differs by 1.3σ. The CPT mass excess result of $-68.1995(94)$ MeV is consistent with ISOLTRAP's result of $-68.1973(29)$ MeV [7]. The recent FRS-ESR measurement disagrees by 2.5σ, with mass excess $-68.521(127)$ MeV [40].

^{141}**Cs:** Neutron-rich cesium isotopes up to ^{142}Cs [3] as well as ^{145,147}Cs [4] have already been measured quite precisely in ISOLTRAP and up to ^{148}Cs with the Orsay double-focusing mass spectrometer [64], also at ISOLDE. Therefore cesium was not investigated extensively in this experiment, with only ^{141,142}Cs measured as a consistency check.

For ^{141}Cs, the AME03 quotes three measurements. Most heavily weighted is the ISOLTRAP measurement of the mass [3], which used ^{133}Cs as the calibrant. The accepted mass of that calibrant had increased between the original paper and the AME03 by 4.7 keV/c^2. By taking this into account the ISOLTRAP mass excess is $-74.475(15)$ MeV, consistent with our value of $-74.466(19)$ MeV.

The other two cited measurements are a β-endpoint measurement of $Q_\beta = 5.242(15)$ MeV [65] and a β-delayed neutron measurement [57]. We can compare with the Q_β measurement by using an earlier CPT measurement of ^{141}Ba [1] to calculate $Q_\beta = 5.274(20)$ MeV, a difference of 1.3σ. We can compare to the AME03 input $Q_{\beta n}$ value of $735(30)$ keV [57] using the similarly adjusted ISOLTRAP mass for ^{140}Ba [3], which yields $752(25)$ keV, in agreement.

^{142}**Cs:** For this nuclide the AME03 considers the ISOLTRAP mass measurement [3] and a Q_β measurement [65] with an additional contribution from the Orsay mass spectrometer [64], with which we cannot make a direct comparison. The adjusted (see ^{141}Cs, above) ISOLTRAP mass excess of $-70.521(15)$ MeV is in agreement with our result of $-70.511(10)$ MeV. Again utilizing previous CPT mass measurements [1], we can calculate Q_β to be $7.340(15)$ MeV, which is 1.2σ from the value from [65] of $7.315(15)$ MeV.

^{153}**Pr:** This mass has previously been measured by the CPT [1] at $152.933\,8895(153)$ u. This is in agreement with the value found in the present experiment of $152.933\,934(39)$ u. The combined CPT result for this nuclide is therefore $152.933\,895(15)$ u. The sole input for the AME03 is a β-endpoint measurement of $5.720(100)$ MeV [66], which agrees with our result of $5.756(15)$ MeV.

155Pr: There are no previous mass measurements of this nuclide, direct or indirect. The AME03 extrapolates a mass excess of $-55.780(300)$ MeV [29], which is 1.2σ from our result of $-55.416(30)$ MeV.

153Nd: There is only one previous mass measurement of this neodymium isotope, a β-endpoint measurement of $Q_\beta = 3.336(25)$ MeV [67], which agrees with our result of $3.306(23)$ MeV.

155Nd: There is also only a single previous measurement of this isotope, a β-endpoint measurement [67] that was discarded by the AME03 due to severe disagreement with systematic trends. That measurement was part of the same experiment as the accurate ^{153}Nd measurement, above. That result of $Q_\beta = 4.222(150)$ MeV is inconsistent with our result of $4.656(18)$ MeV, which is closer to the AME03 interpolated value of $4.500(150)$ MeV [29].

157Nd: The mass of this neodymium isotope has never before been measured by any means, directly or indirectly. The AME03 extrapolates a mass excess of $-56.790(200)$ MeV [29], 1.6σ lighter than this work's $-56.464(43)$ MeV.

153Pm: Three measurements are listed in the AME03. One is a β-endpoint Q-value experiment with a result of $Q_\beta = 1.863(15)$ MeV [67]. No measurement of ^{153}Sm was made by the CPT, but using the well-established AME03 value for that mass the Q_β value is found to be $1.928(23)$ MeV, a 2.4σ difference. A ^{154}Sm$(d,^3{\rm He})^{153}$Pm Q-value measurement of $-3.623(25)$ MeV [45] is also used. Using the well-established mass of ^{154}Sm [29] and our measurement, we find $Q_{(d,^3{\rm He})} = -3.619(23)$ MeV, which is consistent. A different proton-transfer reaction Q value, ^{154}Sm$(t,\alpha)^{153}$Pm [46], was also measured at $10.748(20)$ MeV, which differs from our value of $10.701(25)$ MeV by 1.5σ.

155Pm: The only previous measurement is a β-endpoint measurement of $3.224(30)$ MeV [67], and the CPT result of $3.254(24)$ MeV agrees.

156Pm: Two measurements are listed in the AME03. Both are β-endpoint experiments [66,68], but the CPT has not measured ^{156}Sm so a direct comparison of Q_β is not possible. However, the mass excess determination based on these measurements given by the AME03 of $-64.220(30)$ MeV differs from the CPT value of $-64.1655(59)$ MeV by 1.8σ.

157Pm: The AME03 cites a single β-endpoint measurement for this nuclide, with $Q_\beta = 4.360(100)$ MeV [66]. The CPT measured both parent and daughter, finding $Q_\beta = 4.380(15)$ MeV, which agrees with this value.

158Pm: This has also been measured only by β-endpoint, with a sole experiment in the AME03 giving $Q_\beta = 6.120(100)$ MeV [49]. That experiment has since been re-analyzed by the same group in Hayashi *et al.* [48], resulting in $Q_\beta = 6.085(80)$ MeV. Both values agree with the CPT value of $6.160(26)$ MeV.

159Pm: This nuclide had not been measured by any means as of the AME03 publication, but has since been subject of β-endpoint measurements [50] subsequently reanalyzed by Hayashi *et al.* [48], resulting in $Q_\beta = 5.460(140)$ MeV. This differs from the CPT value of $5.653(21)$ MeV by 1.4σ. The AME03 systematic mass extrapolation gives a mass excess of $-56.850(200)$ MeV, which differs from the CPT value of $-56.557(17)$ MeV by 1.5σ.
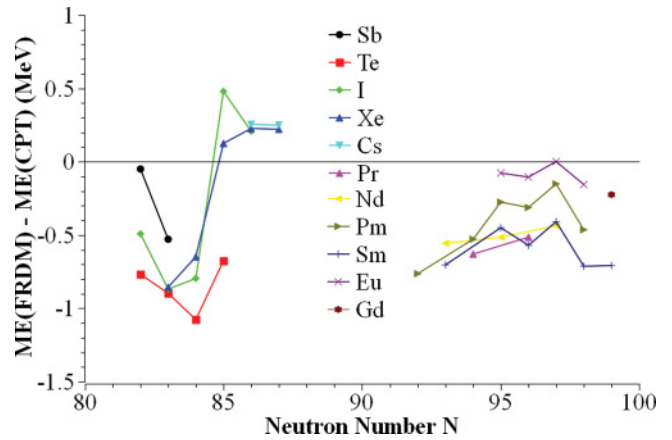

FIG. 9. (Color online) Comparison between CPT measurements and FRDM [73] mass model calculations.
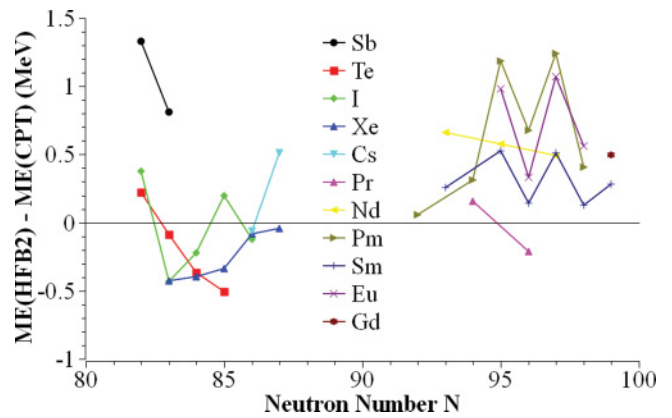

FIG. 10. (Color online) Comparison between CPT measurements and HFB2 [74] mass model calculations.
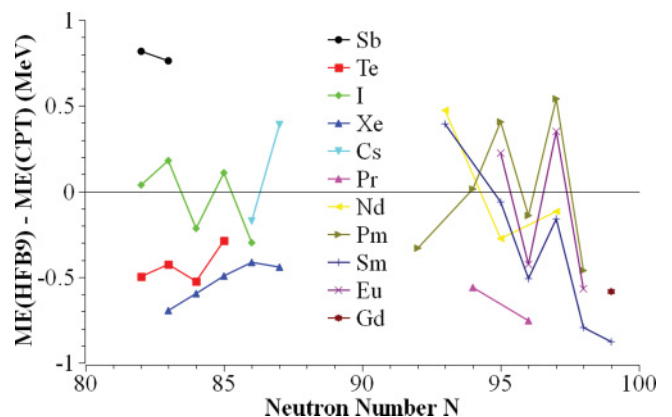

FIG. 11. (Color online) Comparison between CPT measurements and HFB9 [75] mass model calculations.
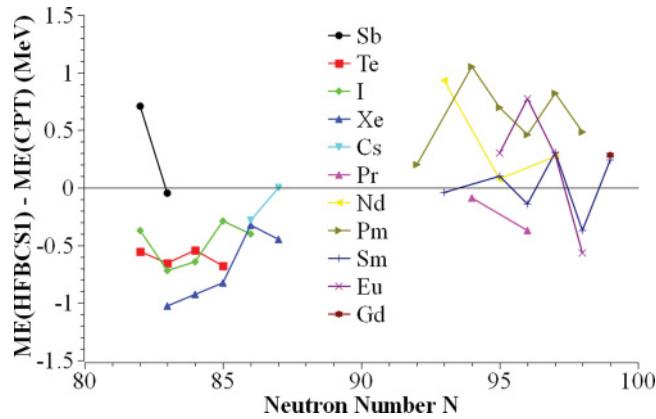
FIG. 12. (Color online) Comparison between CPT measurements and HFBCS1 [76] mass model calculations.
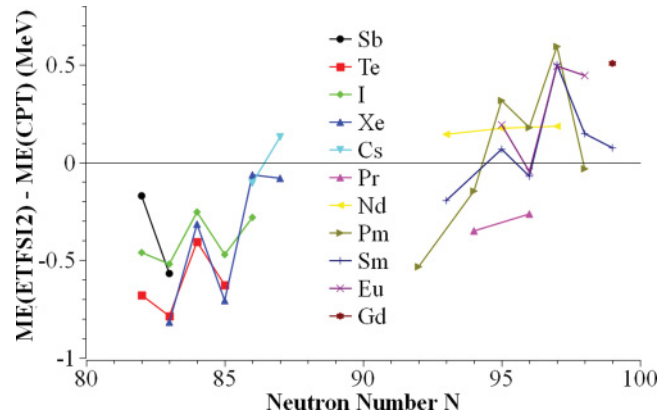

FIG. 15. (Color online) Comparison between CPT measurements and ETFSI2 [79] mass model calculations.
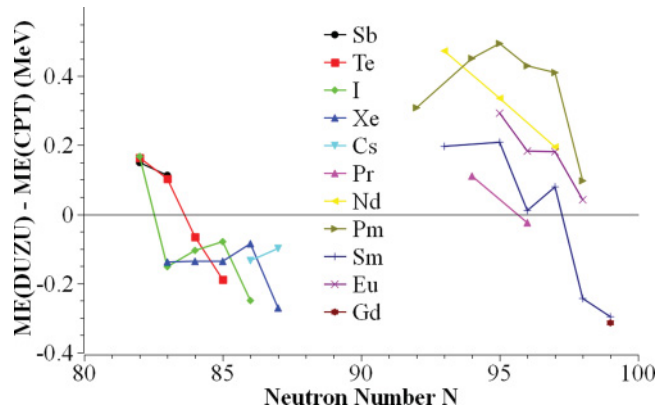

FIG. 13. (Color online) Comparison between CPT measurements and DUZU [77] mass model calculations.
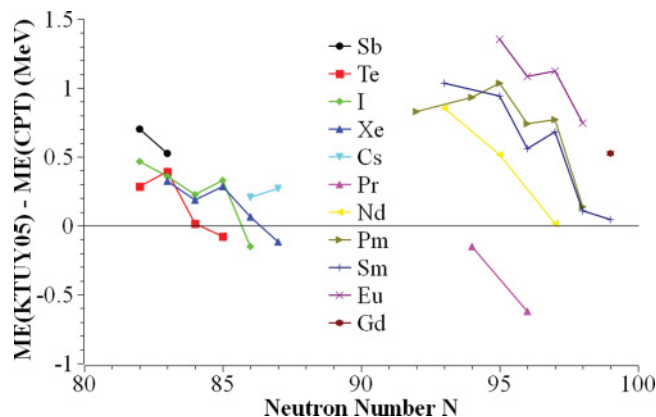

FIG. 14. (Color online) Comparison between CPT measurements and KTUY05 [78] mass model calculations.

^{155}**Sm:** High-precision measurements of the neutron-separation energy of ^{155}Sm have been made in two experiments via the (n, γ) reaction, and these are used exclusively by the AME03 to determine its mass. These measurements were adjusted in the AME03 to $S_n = 5.8068(6)$ MeV [42] and $5.8070(3)$ MeV [43]. By using the well-established AME03 value for the ^{154}Sm mass, the CPT result is $S_n = 5.806(22)$ MeV, which is consistent.

^{157}**Sm:** A single β-endpoint measurement is used in the AME03 determination of this nuclide, with $Q_\beta = 2.734(50)$ MeV [67]. The CPT has not measured the daughter of this decay, so a direct comparison is impossible; however, the CPT mass excess value of $-66.6795(74)$ MeV is consistent with the AME03 value of $-66.730(50)$ MeV.

^{158}**Sm:** A single β-endpoint experiment forms the basis for the AME03 determination of this nuclide's mass, with $Q_\beta = 1.999(15)$ MeV [67], consistent with the CPT value of $2.010(27)$ MeV.

^{159}**Sm:** The AME03 cites a single β-endpoint measurement for this nuclide of $Q_\beta = 3.840(100)$ MeV [49], which has since been reanalyzed by the same group in Hayashi *et al.* [48], resulting in $Q_\beta = 3.805(65)$ MeV. Both values agree with the CPT value of $3.834(14)$ MeV.

^{160}**Sm:** No previous mass measurement of any kind exists for ^{160}Sm. The AME03 extrapolated a mass excess of $-60.420(200)$ MeV, which is consistent with the CPT value of $-60.237(10)$ MeV.

^{161}**Sm:** No measurement of this nuclide existed as of the AME03 publication. It has since been subject of the β-endpoint measurements [50] subsequently reanalyzed by the same group in Hayashi *et al.* [48], who found $Q_\beta = 5.065(130)$ MeV, which agrees with the CPT result of $5.119(23)$ MeV. The CPT mass measurement differs by 310 keV/c^2 with the AME03's extrapolation, which has an uncertainty of 300 keV/c^2.

^{158}**Eu:** This nuclide has two separate β-endpoint measurements, listed in the AME03 as $Q_\beta = 3.550(120)$ [69] and $3.440(100)$ MeV [70], combined in the AME03 to $3.490(80)$ MeV. All of these are consistent with the CPT value of $3.435(25)$ MeV, using the well-established AME03 mass value for ^{158}Gd, which was not measured by the CPT.

[159]**Eu:** This nuclide was the subject of a transfer-reaction experiment, $^{160}Gd(t, \alpha)$, which gave a Q value for that reaction of 10.636(8) MeV [47]. By using the well-known mass of the nearly stable ^{160}Gd from the AME03, the CPT measurement gives $Q_{(t,\alpha)} = 10.622(9)$ MeV, a difference of 1.2σ.

[160]**Eu:** No previous mass measurements for this nuclide were used in the AME03, it having rejected two β-endpoint measurements of $Q_\beta = 3.900(300)$ MeV [71] and 4.200(200) MeV [72]. It has since been the subject of the β-endpoint measurements by Hayashi *et al.,* who found $Q_\beta = 4.705(60)$ MeV [48]. By using the well-known mass of the nearly stable ^{160}Gd from the AME03, the CPT measurement disagrees significantly, with $Q_\beta = 4.467(17)$ MeV, which is 238 keV or 3.8σ from the Hayashi *et al.* result. The CPT mass value is consistent with the AME03 systematic extrapolation.

[161]**Eu:** No previous mass measurement existed for this nuclide as of the AME03 publication, but it has since been the subject of the β-endpoint measurements by Hayashi *et al.,* who found $Q_\beta = 3.705(60)$ MeV [48]. The CPT mass value is consistent with the AME03 systematic extrapolation.

[163]**Gd:** No previous mass measurement existed for this nuclide as of the AME03 publication, but it has since been the subject of the β-endpoint measurements by Hayashi *et al.,* who found $Q_\beta = 3.170(70)$ MeV [48]. The CPT mass value is consistent with the AME03 systematic extrapolation.

B. Mass model comparison

Because most of the r-process path is outside the region of known masses, r-process simulations are forced to use mass models for neutron-separation energy values. Available mass models often disagree significantly for un-

TABLE V. The rms mass-excess difference (σ) and mean mass-excess difference ($\bar{\epsilon}$) of various mass models and the AME03 from the CPT for the measured nuclides presented here.

Model	σ (MeV)	$\bar{\epsilon}$ (MeV)
AME03 [29]	0.171	−0.105
FRDM [73]	0.538	−0.379
HFB2 [74]	0.555	0.281
HFB9 [75]	0.467	−0.175
HFBCS1 [76]	0.546	−0.025
DUZU [77]	0.234	0.062
KTUY05 [78]	0.611	0.438
ETFSI2 [79]	0.396	−0.120

measured masses, so it can be enlightening to compare first-time measurements to mass models which were created before these masses were available. Table V summarizes the overall precision and accuracy of, and Figs. 9–15 compare the new CPT measurements to, various popular mass models.

The finite-range droplet model (FRDM) is a commonly used model for r-process simulations, and a comparison with the new CPT results is shown in Fig. 9. The $N = 82$ shell closure is followed by an oscillation about the true masses at higher N, though these oscillations appear to be damped away by $N = 95$. This region is important for the r process, because its path is expected to exit the $N = 82$ shell after the possible ^{130}Cd waiting point [12]. If the overshooting in binding energy past $N = 82$ continues for Z lower than measured here, then the location of the r-process path may be closer to stability for $Z = 49$ and 50 than the FRDM would indicate. Clearly more mass measurements around $Z = 49$ and 50 are vital for an accurate path determination past $N = 82$.
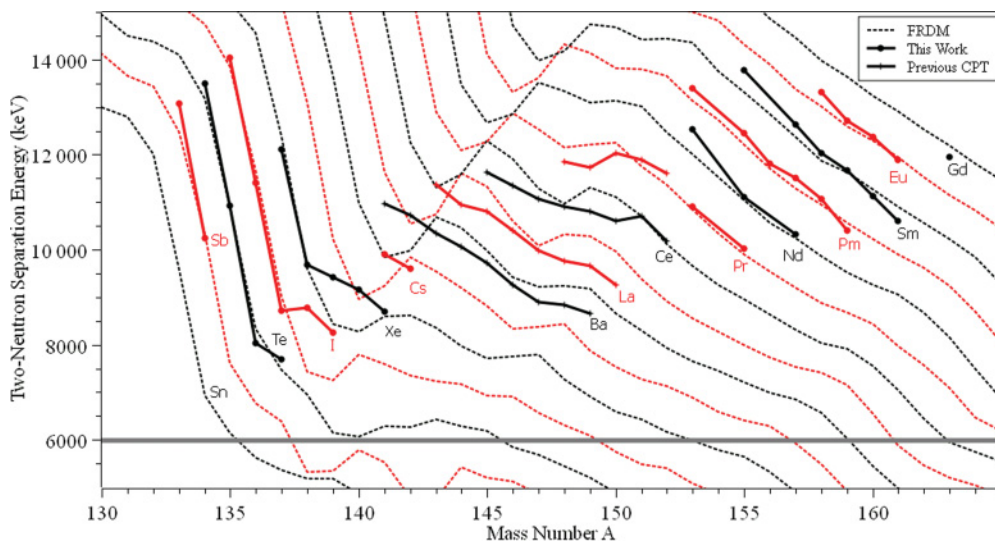

FIG. 16. (Color online) Comparison between two-neutron separation energies for CPT measurements and the FRDM mass model calculations which have frequently been used for astrophysics simulations. Colors alternate with Z for clarity. The first two points for each element include one AME03 mass value each to determine S_{2n}, while the rest use only CPT data. The crosses represent previously published CPT measurements [1]. The r-process path is thought to lie near $S_{2n} \approx 6000$ keV, as indicated by the gray line.

For astrophysics modeling it is not the absolute errors in mass models that are relevant but systematically increasing errors with N, because this is what affects S_n and thus the process paths. For example, Table V would suggest that the Duflo and Zuker (DUZU) model is one of the most accurate in this region, but Fig. 13 shows that for most elements the deviations from our results have negative slope at 50 to 100 keV per neutron. Given the S_n slope of DUZU here, the difference in S_n corresponds to a shift in the r-process path of about one neutron closer to stability were the S_n difference to continue changing with the same slope. The model of Koura, Tachibana, Uno, and Yamada (KTUY05) (Fig. 14) shows the same trend but with even larger magnitude. An Extended Thomas-Fermi plus Strutinsky Integral based model (ETFSI2) (Fig. 15) on the other hand has a slope of similar magnitude in the opposite direction. Any such trend in Hartree-Fock-Bogoliubov models HFB2 and HFB9 (Figs. 10 and 11) is harder to identify given the apparent difficulty with pairing effects at large N, with many changes of over 500 keV in mass deviation from isotope to isotope. The Hartree-Fock-BCS (HFBCS1) model (Fig. 12) had the lowest mean mass difference from the CPT among these models, but it had among the largest scatters in difference, spanning over 2 MeV.

Figure 16 compares neutron separation energies for the CPT and FRDM and suggests a more complicated story for this model. Of course, these new measurements are still very far from the predicted r-process path, so reliable predictions of the path location are not yet possible. Given the varied problems with mass models, forming any expectation that one would be more accurate than the others at yet higher neutron excess would be a gamble. It is clear that mass measurements on or close to the r-process path are sorely needed, especially at the $N = 82$ waiting points.

V. SUMMARY AND OUTLOOK

Mass measurements of 40 nuclides were made, most of which improved the precision and accuracy over literature values. Results are largely consistent with previous results from Penning traps, reaction energetics, and storage ring measurements, but they are frequently much lower in mass than results from β-endpoint measurements. Comparison with mass models shows only sporadic agreement and suggests unsuitability of these models for precise astrophysical r-process simulations. Reliable mass measurements yet closer to and on the r-process path are still needed.

The CPT has been moved to the new CAlifornium Rare Isotope Breeder Upgrade (CARIBU) facility [80] now operating at the ATLAS accelerator and a successor campaign to these measurements has begun. The extent of the CPT's previous measurements was limited by the purity and rate of the available beam, and CARIBU offers several improvements over the system used here to overcome these limitations. The 10^3–10^4 times more intense fission source and larger gas catcher will allow access to nuclides 3–5 neutrons farther from stability. A new compact higher-resolution in-flight isobar separator [81] promises purification with a resolving power of 20 000—four times that of the previous system—while avoiding the saturation of ion traps that would have occurred otherwise with such an intense beam. The in-flight separation will also defer the limitation in nuclide lifetime that would be imposed by in-trap purification. Many of the newly available nuclides lie directly on potential r-process paths near $Z = 50$. The CPT will be used to conduct a survey of all accessible r-process nuclides in this vicinity, as well as any other neutron-rich species made available with the goal of finding isomers, regions of deformation, and shell quenching. Over 200 additional masses are expected to be measured using the CPT.

[1] G. Savard *et al.*, Int. J. Mass Spectrom. **251**, 252 (2006).

[2] C. Rauth *et al.*, Eur. Phys. J. Special Top. **150**, 329 (2007).

[3] F. Ames *et al.*, Nucl. Phys. A **651**, 3 (1999).

[4] C. Weber, G. Audi, D. Beck, K. Blaum, G. Bollen, F. Herfurth, A. Kellerbauer, H.-J. Kluge, D. Lunney, and S. Schwarz, Nucl. Phys. A **803**, 1 (2008).

[5] U. Hager *et al.*, Phys. Rev. Lett. **96**, 042504 (2006).

[6] U. Hager *et al.*, Phys. Rev. C **75**, 064302 (2007).

[7] D. Neidherr *et al.*, Phys. Rev. C **80**, 044323 (2009).

[8] S. Ettenauer *et al.*, Phys. Rev. C **81**, 024314 (2010).

[9] G. Bollen and S. Schwarz, J. Phys. B **36**, 941 (2003).

[10] K. Blaum, Yu. N. Novikov, and G. Werth, Contemp. Phys. **51**, 149 (2010).

[11] E. M. Burbidge, G. R. Burbidge, W. A. Fowler, and F. Hoyle, Rev. Mod. Phys. **29**, 547 (1957).

[12] J. J. Cowan, F.-K. Thielemann, and J. W. Truran, Phys. Rep. **208**, 267 (1991).

[13] M. Arnould, S. Goriely, and K. Takahashi, Phys. Rep. **450**, 97 (2007).

[14] A. Arcones and G. Martínez-Pinedo, Phys. Rev. C **83**, 045809 (2011).

[15] K. Farouqi, K.-L. Kratz, B. Pfeiffer, T. Rauscher, F.-K. Thielemann, and J. W. Truran, Astrophys. J. **712**, 1359 (2010).

[16] S. Wanajo, S. Goriely, M. Samyn, and N. Itoh, Astrophys. J. **606**, 1057 (2004).

[17] R. Fossion, C. De Coster, J. E. García-Ramos, T. Werner, and K. Heyde, Nucl. Phys. A **697**, 703 (2002).

[18] I. Dillmann *et al.*, Phys. Rev. Lett. **91**, 162503 (2003).

[19] J. Fallis, Ph.D. thesis, University of Manitoba, 2009, [http://hdl.handle.net/1993/3210].

[20] G. Savard *et al.*, Nucl. Instrum. Methods B **204**, 582 (2003).

[21] M. Wada *et al.*, Nucl. Instrum. Methods B **204**, 570 (2003).

[22] F. Herfurth *et al.*, Nucl. Instrum. Methods A **469**, 254 (2001).

[23] G. Savard, St. Becker, G. Bollen, H.-J. Kluge, R. B. Moore, Th. Otto, L. Scweikhard, H. Stolzenberg, and U. Wiess, Phys. Lett. A **158**, 247 (1991).

[24] S. Brown and G. Gabrielse, Rev. Mod. Phys. **58**, 233 (1986).

[25] G. Bollen, R. B. Moore, G. Savard, and H. Stolzenberg, J. Appl. Phys. **68**, 4355 (1990).

[26] M. König, G. Bollen, H.-J. Kluge, T. Otto, and J. Szerypo, Int. J. Mass Spectrom. Ion Process. **142**, 95 (1995).

[27] J. A. Clark, Ph.D. thesis, University of Manitoba, 2005 [http://hdl.handle.net/1993/177].

[28] M. Redshaw, E. Wingfield, J. McDaniel, and E. G. Myers, Phys. Rev. Lett. **98**, 053003 (2007).

[29] A. H. Wapstra, G. Audi, and C. Thibault, Nucl. Phys. A **729**, 129 (2003); G. Audi, A. H. Wapstra, and C. Thibault, *ibid.* **729**, 337 (2003).

[30] P. G. Wenthold, J. A. Paulino, and R. R. Squires, J. Am. Chem. Soc. **113**, 7414 (1991).

[31] X. Zhang and P. Chen, J. Am. Chem. Soc. **114**, 3147 (1992).

[32] M. W. Chase, *NIST-JANAF Thermochemical Tables* (American Chemical Society, Washington,1998), Vol. 1, p. 551, Vol. 2, p. 1261.

[33] N. D. Scielzo *et al.*, Phys. Rev. C **80**, 025501 (2009).

[34] G. Gabrielse, Int. J. Mass Spectrom. **279**, 107 (2009).

[35] G. Bollen, H.J. Kluge, M. Konig, T. Otto, G. Savard, H. Stolzenberg, R. B. Moore, G. Rouleau, G. Audi, and ISOLDE Collaboration, Phys. Rev. C **46**, 2140(R) (1992).

[36] A. Korgul *et al.*, Eur. Phys. J. A **15**, 181 (2002).

[37] J. Shergur, A Wöhr, W. B. Walters, K.-L. Kratz, O. Arndt, B. A. Brown, J. Cederkall, I. Dillmann, L. M. Fraile, P. Hoff, A. Joinet, U. Köster, and B. Pfeiffer, Phys. Rev. C **71**, 064321 (2005).

[38] U. Keyser, H. Berg, F. Münnich, B. Pahlman, K. Hawerkamp, B. Pfeiffer, H. Schrader, and E. Monnand, in *Atomic Masses and Fundamental Constants, 6*, edited by J. A. Nolen Jr. and W. Benenson (Plenum Press, New York, 1980), p. 485.

[39] J. Fallis *et al.*, Phys. Rev. C **84**, 045807 (2011).

[40] B. Sun *et al.*, Nucl. Phys. A **812**, 1 (2008).

[41] R. B. Firestone, S. F. Mughabghab, and G. L. Molnár, IAEA Tech. Doc. STI/PUB/1263, 2007.

[42] I. F. Barchuk, V. I. Golyshkin, and E. N. Gorban, Izv. Akad. Nauk SSSR, Ser. Fiz. **46**, 63 (1982).

[43] K. Schreckenbach *et al.*, Nucl. Phys. A **376**, 149 (1982).

[44] B. H. Wildenthal, E. Newman, and R. L. Auble, Phys. Rev. C **3**, 1199 (1971).

[45] E. Sugarbaker and W. S. Gray, Bull. Am. Phys. Soc. **21**, 984 (1976).

[46] D. G. Burke, G. Løvhøiden, E. R. Flynn, and J. W. Sunier, Phys. Rev. C **18**, 693 (1978).

[47] D. G. Burke, G. Løvhøiden, E. R. Flynn, and J. W. Sunier, Nucl. Phys. A **318**, 77 (1979).

[48] H. Hayashi *et al.*, Eur. Phys. J. A **34**, 363 (2007).

[49] M. Shibata, T. Shindou, Y. Kojima, M. Asai, K. Tsukada, S. Ichikawa, H. Haba, Y. Nagame, and K. Kawade, Japan Atomic Energy Research Institute, Tandem VDG Annual Report, 2001 (2002) p. 26 JAERI-Review 2002-029 (2002).

[50] M. Shibata, O. Suematsu, K. Kawade, M. Asai, S. Ichikawa, Y. Nagame, A. Osa, K. Tsukada, Y. Kojima, and A. Taniguchi, Japan Atomic Energy Research Institute, Tandem VDG Annual Report, 2002 (2003) p. 32 JAERI-Review 2003-028 (2003).

[51] B. Fogelberg, K. A. Mezilev, V. I. Isakov, K. I. Erokhina, H. Mach, E. Ramström, and H. Gausemel, Phys. Rev. C **75**, 054308 (2007).

[52] M. Shibata, Y. Kojima, H. Uno, K. Kawade, A. Taniguchi, Y. Kawase, S. Ichikawa, F. Maekawa, and Y. Ikeda, Nucl. Instrum. Methods A **459**, 581 (2001).

[53] B. Fogelberg, K. A. Mezilev, H. Mach, V. I. Isakov, and J. Slivova, Phys. Rev. Lett. **82**, 1823 (1999).

[54] K. A. Mezilev, Yu. N. Novikov, A. V. Popov, B. Fogelberg, and L. Spanier, Phys. Scr., T **56**, 272 (1995).

[55] M. Graefenstedt, U. Keyser, F. Münnich, and F. Schreiber, AIP Conf. Proc. **164**, 30 (1987).

[56] M. Samri, G. J. Costa, G. Klotz, D. Magnac, R. Seltz, and J. P. Zirnheld, Z. Phys. A **321**, 255 (1985).

[57] K.-L. Kratz, A. Schröeder, H. Ohm, H. Gabelmann, W. Ziegert, B. Steinmüller, and B. Pfeiffer, in *Proceedings of the 7th International Conference on Atomic Masses and Fundamental Constants AMCO-7*, edited by O. Klepper (Technishe Hochschule Darmstadt Lehrdruckerei, Darmstadt, 1984), p. 127.

[58] F. Schussler, J. Blachot, E. Monnand, J. A. Pinston, and B. Pfeiffer, Z. Phys. A **283**, 43 (1977).

[59] E. Lund and G. Rudstam, Nucl. Instrum. Methods **134**, 173 (1976).

[60] N. R. Johnson and G. D. O'Kelley, Phys. Rev. **114**, 279 (1959).

[61] M. Groß, P. Jürgens, U. Keyser, S. Kluge, M. Mehrtens, S. Müller, F. Münnich, J. Wulff, and H. R. Faust, Nucl. Instrum. Methods A **311**, 512 (1992).

[62] E. Monnand, R. Brissot, L. C. Carraz, J. Crançon, C. Ristori, F. Schussler, and A. Moussa, Nucl. Phys. A **195**, 192 (1972).

[63] F. K. Wohn and W. L. Talbert Jr., Phys. Rev. C **18**, 2328 (1978).

[64] G. Audi, A. Coc, M. Epherre-Rey-Campagnolle, G. Le Scornet, C. Thibault, and F. Touchard, Nucl. Phys. A **449**, 491 (1986).

[65] M. Przewloka, A. Przewloka, P. Wächter, and H. Wollnik, Z. Phys. A **342**, 27 (1992).

[66] M. Shibata, T. Shindou, K. Kawade, Y. Kojima, A. Taniguchi, Y. Kawase, and S. Ichikawa, in *Exotic Nuclei and Atomic Masses, ENAM2001*, edited by J. Äystö, P. Dendooven, A. Jokinen, and M. Leino (Springer-Verlag, Berlin, Heidelberg, 2001), p. 479.

[67] R. C. Greenwood and M. H. Putnam, Nucl. Instrum. Methods A **337**, 106 (1993).

[68] M. Hellström, B. Fogelberg, L. Spanier, and H. Mach, Phys. Rev. C **41**, 2325 (1990).

[69] F. Schima and T. Katoh, Phys. Rev. **140**, B1496 (1965).

[70] W. R. Daniels and D. C. Hoffman, Phys. Rev. **147**, 845 (1966).

[71] J. M. D'Auria, R. D. Guy, and S. C. Gujrathi, Can. J. Phys. **51**, 686 (1973).

[72] N. A. Morcos, W. D. James, D. E. Adams, and P. K. Kuroda, J. Inorg. Nucl. Chem. **35**, 3659 (1973).

[73] P. Möller, J. R. Nix, W. D. Myers, and W. J. Swiatecki, At. Data Nucl. Data Tables **59**, 185 (1995).

[74] S. Goriely, M. Samyn, P.-H. Heenen, J. M. Pearson, and F. Tondeur, Phys. Rev. C **66**, 024326 (2002).

[75] S. Goriely, M. Samyn, J. M. Pearson, and M. Onsi, Nucl. Phys. A **750**, 425 (2005).

[76] F. Tondeur, S. Goriely, J. M. Pearson, and M. Onsi, Phys. Rev. C **62**, 024308 (2000).

[77] J. Duflo and A. P. Zuker, Phys. Rev. C **52**, R23 (1995).

[78] H. Koura, T. Tachibana, M. Uno, and M. Yamada, Prog. Theor. Phys. **113**, 305 (2005).

[79] S. Goriely, AIP Conf. Proc. **529**, 287 (2000).

[80] G. Savard, S. Baker, C. Davids, A. F. Levand, E. F. Moore, R. C. Pardo, R. Vondrasek, B. J. Zabransky, and G. Zinkann, Nucl. Instrum. Methods B **266**, 4086 (2008).

[81] C. N. Davids and D. Peterson, Nucl. Instrum. Methods B **266**, 4449 (2008).